Quantum efficiency of photoemission from biased metal surfaces with laser wavelengths from UV to NIR

Cite as: J. Appl. Phys. **130**, 064902 (2021); https://doi.org/10.1063/5.0059497
Submitted: 09 June 2021 . Accepted: 24 July 2021 . Published Online: 12 August 2021

Yang Zhou, and Peng Zhang

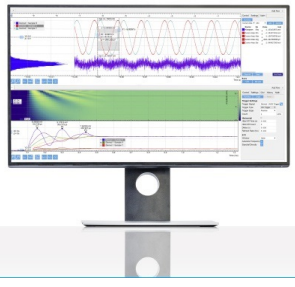

Journal of Applied Physics ARTICLE scitation.org/journal/jap

Quantum efficiency of photoemission from biased metal surfaces with laser wavelengths from UV to NIR

Cite as: J. Appl. Phys. **130**, 064902 (2021); doi: 10.1063/5.0059497
Submitted: 9 June 2021 · Accepted: 24 July 2021 ·
Published Online: 12 August 2021

Yang Zhou and Peng Zhang[a)]

AFFILIATIONS

Department of Electrical and Computer Engineering, Michigan State University, East Lansing, Michigan 48824-1226, USA

[a)]**Author to whom correspondence should be addressed:** pz@egr.msu.edu

ABSTRACT

This paper studies photoelectron emission from metal surfaces with laser wavelengths from 200 to 1200 nm (i.e., ultraviolet to near-infrared), using a recent quantum model based on the exact solution of time-dependent Schrödinger equation. The dominant electron emission mechanism varies from different multiphoton emission processes to dc or optical field emission, depending on the laser intensity, wavelength, and dc bias field. The parametric dependence of the quantum efficiency (QE) is analyzed in detail. It is found that QE can be increased nonlinearly by the non-equilibrium electron heating produced by intense sub-picosecond laser pulses. This increase of QE due to laser heating is the strongest near laser wavelengths where the cathode work function is an integer multiple of the corresponding laser photon energy. The quantum model, with laser heating effects included, reproduces previous experimental results, which further validates our quantum model and the importance of laser heating.

I. INTRODUCTION

Laser-induced photoemission is important to a variety of advanced applications, such as photocathodes for free electron lasers,[1–3] bright x-ray sources,[4] ultrafast electron microscopy,[5–9] carrier-envelope detection,[10,11] strong-field nano-optics,[12–14] and novel nano-electronic devices.[15–20] Photoemission processes have been studied extensively over a wide range of laser wavelengths, both experimentally and theoretically. Single-photon photoemission process and the nonlinearity in strong laser intensity range due to the laser heating effect have been observed in the ultraviolet (UV) wavelength range for various metallic cathodes.[21–25] Laser of wavelength around 800 nm has been widely used, and multiple photoemission mechanisms, including multiphoton absorption, above-threshold photoemission, photo-assisted field emission, and optical field tunneling,[26–32] have been reported. With laser wavelengths from 1 to 1.5 μm, Park *et al.*[33] observed the narrowing of the emission cone angle of the fastest electrons when laser intensity increases, which is ascribed to field-induced steering of subcycle electrons. Few-cycle mid-infrared (up to 8 μm) laser pulses are applied to single plasmonic nanotips, and it is found that the electrons can escape the local field within a fraction of an optical half-cycle.[34] Single-cycle terahertz pulses have also been demonstrated to have their capacity to control nanotip photoemission electron dynamics.[35]

Classical models, such as the three-step model and the Fowler–DuBridge model,[23,24,36–42] mainly focus on single-photon (or photon energy $\hbar\omega >$ work function W, mostly in UV) photoemission. The Fowler–DuBridge model has also been extended to include multiphoton emission and photo-thermionic emission processes;[43–47] however, the multiphoton emission coefficients typically require empirical fitting, and the model's validity is questionable when applying to strong-field regimes.[48] Yalunin *et al.*[49] theoretically treat photoemission from metal surfaces by perturbation theory, the Floquet method, and the Crank–Nicolson numerical approach. Despite extensive studies on photoemission by lasers of a wide wavelength range, there is still lack of systematic analysis on the effects of laser wavelength on photoemission and the corresponding quantum efficiency.

In this paper, we study the photoemission current density and quantum efficiency over a wide range of laser wavelengths from 200 to 1200 nm, using a recent quantum model based on the exact solution of time-dependent Schrödinger equation.[50] We examine

the laser heating effects on photoemission by using the two-temperature model (TTM),[51,52] in which electrons and the lattice are treated in separate thermal equilibrium and are characterized by their own temperatures. TTM is found to be suitable for laser pulses on a time scale of a few hundreds of femtoseconds to tens of picosecond.[21,22,53–56] Our results show that the laser heating induced electron redistribution can enhance photoemission quantum efficiency, especially at laser wavelengths where the ratio of work function of cathode to photon energy is close to an integer.

II. PHOTOEMISSION WITHOUT LASER HEATING EFFECTS

A. Brief description of the quantum model

The quantum model of photoemission is constructed by solving the time-dependent Schrödinger equation, which is applicable to arbitrary laser electric fields (strength and wavelength), cathode properties (any Fermi level and work function), and dc electric field.[31,50] The work has been extended to two-color laser-induced photoemission[32,57,58] and to few-cycle pulsed laser excitation[11] with excellent agreement with experiments. This quantum model has been corroborated by comparing with classical models, i.e., the three-step model and the Fowler–DuBridge model,[50] and has been applied to plasmonic enhanced photoemission from nanotips.[59]

The one-dimensional (1D) quantum model considers electron emission from a flat metal surface under the action of a laser electric field $F_1 \cos \omega t$ and a dc electric field F_0. Both dc and laser fields are assumed to be perpendicular to the metal surface, which has a Fermi energy E_F, effective work function with the Schottky effect[60] of $W = W_0 - 2\sqrt{e^3 F_0/16\pi\varepsilon_0}$, where W_0 is the nominal work function, e is the (positive) elementary charge, and ε_0 is the free space permittivity.

Based on the exact solution of time-dependent Schrödinger equation subject to the oscillatory surface barrier due to the dc and laser fields,[31,50] the time-averaged electron transmission probability from energy level of ε is obtained as

$$D(\varepsilon) = \sum_{n=-\infty}^{\infty} w_n(\varepsilon), \tag{1}$$

where $w_n(\varepsilon)$ denotes the electron transmission probability through n-photon process, with $n<0$ representing multiphoton emission process, $n=0$ direct tunneling process, and $n>0$ multiphoton absorption process. The detailed expressions for $w_n(\varepsilon)$ can be found in Refs. 31 and 50.

The total emission current density is a sum of electron emission from all the electron initial energies ε available inside the cathode, which is given as

$$J = e\int_0^{\infty} D(\varepsilon)N(\varepsilon)d\varepsilon, \tag{2}$$

where $D(\varepsilon)$ is given in Eq. (1), $N(\varepsilon) = \frac{mk_BT}{2\pi^2\hbar^3}\ln\left[1+\exp\left(\frac{E_F-\varepsilon}{k_BT}\right)\right]$ is the supply function with $N(\varepsilon)d\varepsilon$ representing the number of electrons inside the cathode impinging normal to the cathode surface with longitudinal energy between ε and $\varepsilon + d\varepsilon$ across unit area per unit time, assuming Fermi–Dirac distribution of the electrons in the metal,[50,61–63] k_B is the Boltzmann constant, and T is the temperature.

Following our previous work,[50] the quantum efficiency (QE) of photoemission is defined as the ratio of the number of emitted electrons to that of the incident photons,

$$\mathrm{QE} = \frac{J/e}{I/\hbar\omega}, \tag{3}$$

where J is the emission current density given in Eq. (2) and $I = \varepsilon_0 c F_1^2/2$ is the incident (propagating parallel to the 1D surface), linearly polarized laser intensity, with c the light speed in the vacuum.

B. Transmission probability

Figure 1 shows the time-averaged transmission probability $w_n(\varepsilon = E_F)$ through the nth channel (or n-photon process) under various combinations of dc electric field F_0, laser electric field F_1, and laser wavelength λ ($= 2\pi c/\omega$). The metal is assumed to be gold with Fermi energy of $E_F = 5.53$ eV and work function of $W_0 = 5.1$ eV. Unless specified otherwise, these are the default cathode properties in this study. The laser wavelengths are 200, 400, 800, and 1200 nm, corresponding to the photon energy of 6.20, 3.10, 1.55, and 1.03 eV, respectively. The laser fields F_1 for lines in red, green, blue, and purple are 0.1, 1, 3, and 6 V/nm, corresponding to the local laser intensity of 1.33×10^9, 1.33×10^{11}, 1.20×10^{12}, and 4.79×10^{12} W/cm^2, respectively. The electron initial longitudinal energy is assumed to be at the Fermi level, i.e., $\varepsilon = E_F$. It is obvious that the electron transmission probability $w(E_F)$ increases when the laser field increases. For $F_1 = 6$ V/nm, there is more contribution from the large values of nth channel to the total transmission probability, especially for the cases of $\lambda = 800$ and 1200 nm. When $F_0 = 0$, the dominant emission process for $\lambda = 200$, 400, 800, and 1200 nm are one-, two-, four-, and five-photon absorption processes, respectively. This is consistent with the integer value of $\langle W/\hbar\omega + 1\rangle$, with $\langle\rangle$ denoting the integer part of the expression. It is interesting to observe that the dominant channel shifts from $n=5$ to $n=6$ for $\lambda = 1200$ nm, when F_1 increases to 3 and 6 V/nm [Fig. 1(d)] due to the channel closing effect,[64] where the to-be-liberated electrons have to overcome not only the potential barrier but also the ponderomotive energy $U_p = e^2F_1^2/4m\omega^2$ in the laser field[28] such that the electron drift kinetic energy $E_n = \varepsilon + n\hbar\omega - E_F - W - U_p$ is larger than zero. A small dc field $F_0 = 0.1$ V/nm has little effect on the transmission probability for $\lambda = 200$ and 400 nm [Figs. 1(e) and 1(f)]. However, it shifts the dominant channel from $n=4$ to $n=3$ for $\lambda = 800$ nm when $F_1 = 0.1$, 1, and 3 V/nm [Fig. 1(g)] and also shifts the dominant channel from $n=6$ to $n=5$ for $\lambda = 1200$ nm when $F_1 = 3$ and 6 V/nm [Fig. 1(h)]. This is due to the lowering of the surface potential barrier by the dc electric field, therefore lowering the number of photons required to overcome the barrier. When $F_0 = 1$ V/nm, more nth channels of lower order are opened up, and the dominant channel is further shifted to smaller value of nth channels, especially for $\lambda = 400$, 800, and

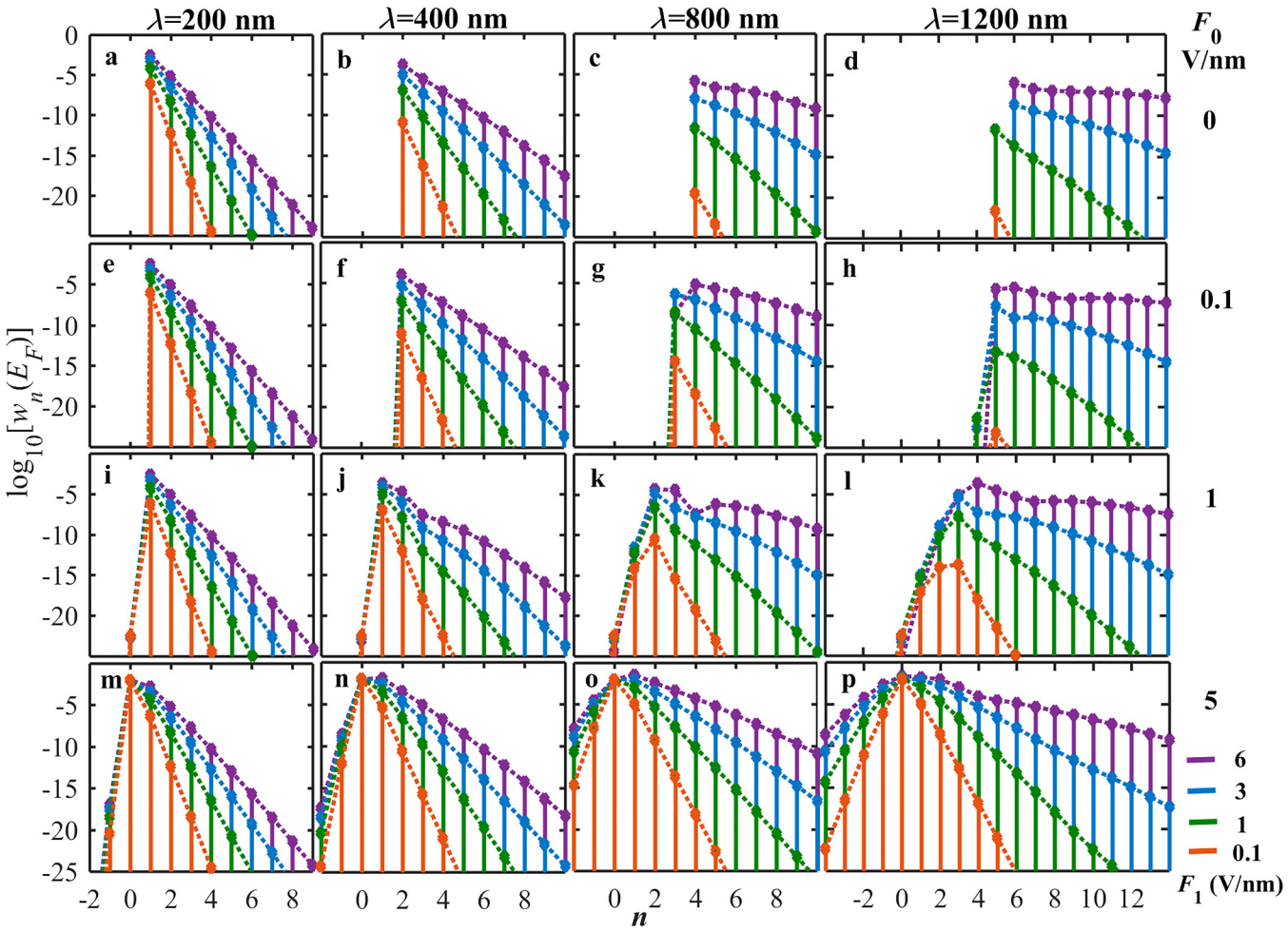

FIG. 1. Electron transmission probability from initial longitudinal energy of E_F through nth channel under various combinations of dc electric field F_0, laser field F_1, and laser wavelength λ. (a)–(d) $F_0 = 0$ V/nm; (e)–(h) $F_0 = 0.1$ V/nm; (i)–(l) $F_0 = 1$ V/nm; and (m)–(p) $F_0 = 5$ V/nm. In each column, (a), (e), (i), and (m) $\lambda = 200$ nm; (b), (f), (j), and (n) $\lambda = 400$ nm; (c), (g), (k), and (o) $\lambda = 800$ nm; and (d), (h), (l), and (p) $\lambda = 1200$ nm. The laser fields F_1 corresponding to lines in red, green, blue, and purple are 0.1, 1, 3, and 6 V/nm, respectively. The metal is assumed to be gold with $E_F = 5.53$ eV and $W_0 = 5.1$ eV.

1200 nm [Figs. 1(j)–1(l)]. When $F_0 = 5$ V/nm, the dominant emission process is direct field tunneling, i.e., through $n = 0$, regardless of the laser wavelength.

The electron transmission probability $D(\varepsilon)$ as a function of electron longitudinal energy ε and laser wavelength λ, under various combinations of dc electric field F_0 and laser field F_1, is shown in Fig. 2. When $F_0 = 0$, the three-dimensional (3D) surface plot shows stair-like behavior as a function of ε for a given λ [Figs. 2(a)–2(d)]. Each stair corresponds to n-photon absorption process, with n increasing as ε decreases, for a given λ. As F_1 increases, the electron transmission probability increases and more "stairs" clearly appear at the bottom right region, i.e., the "smaller initial energy"–"longer laser wavelength" region. When $F_0 = 1$ V/nm, the electron transmission probability is increased due to the lowering of the surface potential barrier. The step edge between "stairs" is not as steep as that with zero dc field but becomes gradual [Figs. 2(e)–2(h)]. Dc electric field has a greater enhancement on the emission induced by a longer wavelength laser.[50] This can be explained by the change of the dominant emission process, which shifts to smaller n-photon absorption process due to the lowering of the surface potential barrier by the applied dc field. From Figs. 1(a)–1(d), it can be observed that the $(n+1)$-photon absorption process has a probability orders of magnitude lower than the n-photon absorption process for a given λ. When $F_0 = 5$ V/nm, the 3D surface plot of $D(\varepsilon)$ becomes smooth [Figs. 2(i)–2(l)]. At each electron initial longitudinal energy ε, $D(\varepsilon)$ is almost constant for all different laser wavelengths, which implies that the dominant emission process is due to the dc field tunneling, consistent with Figs. 1(m)–1(p). In Figs. 2(i)–2(l), as the laser field F_1 increases from 0.1 to 6 V/nm, $D(\varepsilon)$ increases and the stair shape

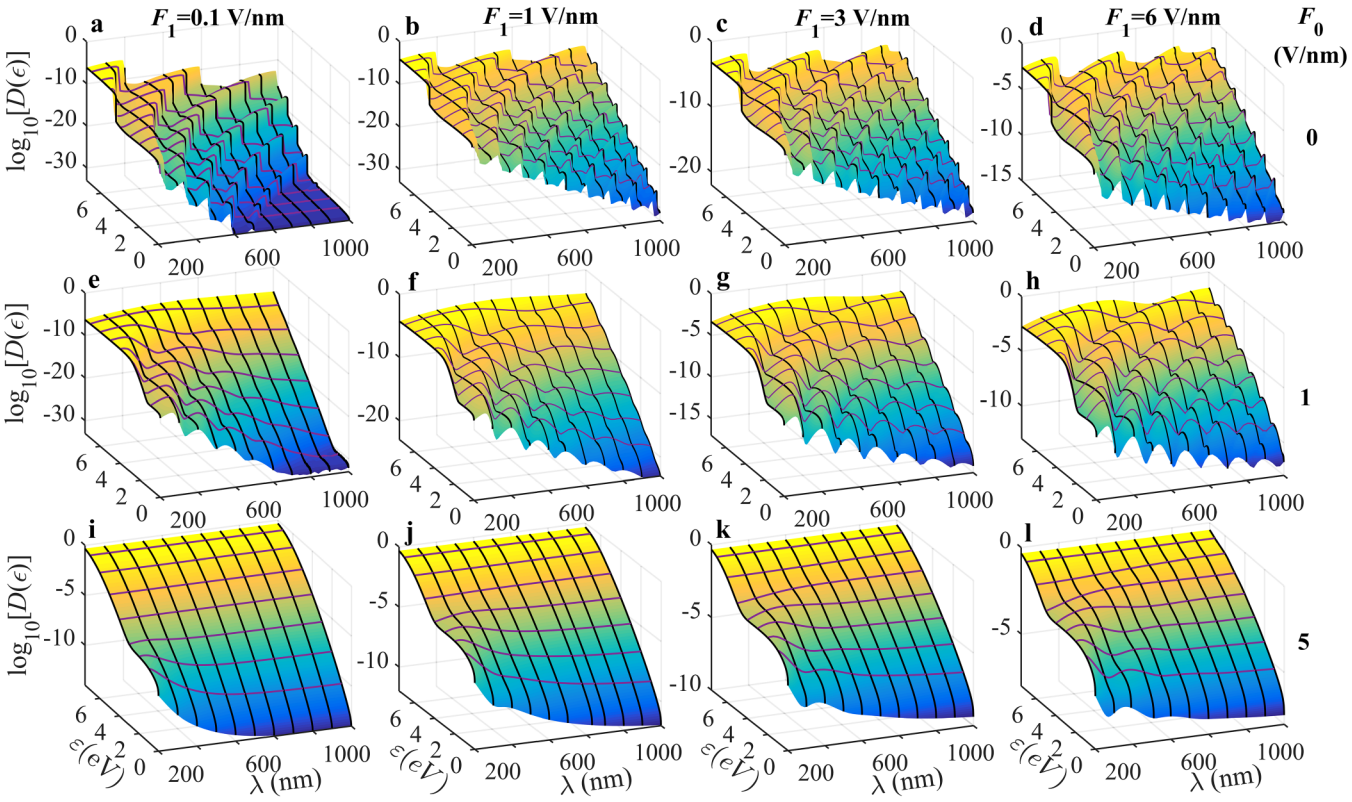

FIG. 2. Electron transmission probability $D(\varepsilon)$ as a function of electron initial energy ε and laser wavelength λ for various combinations of laser field F_1 and dc electric field F_0. (a)–(d) $F_0 = 0$ V/nm; (e)–(h) $F_0 = 1$ V/nm; and (i)–(l) $F_0 = 5$ V/nm. In each column, (a), (e), and (i) $F_1 = 0.1$ V/nm; (b), (f), and (j) $F_1 = 1$ V/nm; (c), (g), and (k) $F_1 = 3$ V/nm; and (d), (h), and (l) $F_1 = 6$ V/nm.

of the surface in the shorter wavelength range becomes more obvious. The shape of the 3D surfaces is determined by the relative strength of laser and dc electric fields.

Figure 3 shows the electron transmission probability $D(\varepsilon = E_F)$ as a function of laser wavelength under various combinations of dc and laser electric fields, which is the projection of $D(\varepsilon)$ in the $D-\lambda$ plane with $\varepsilon = E_F$ in Fig. 2. When $F_0 = 0$, the curves display distinct stair shape, though each step is not flat, especially for $\lambda > 486$ nm, i.e., $n = W_0/\hbar\omega > 2$. For small F_1, $D(E_F)$ has its maximum value at the step point in each step, corresponding to an integer value of the ratio of $W_0/\hbar\omega$. As the laser field F_1 increases, $D(E_F)$ is enhanced greatly, especially for $\lambda > 486$ nm. This is because $D(\varepsilon = E_F) \propto F_1^{2n}$ in the n-photon photoemission regime. Meanwhile, the step points shift to smaller laser wavelength when F_1 gets larger, which is indicated by the dashed arrow line in Fig. 3(a). This shift is due to the channel closing effect, which is more pronounced for longer laser wavelength. When there is a small dc electric field ($F_0 = 0.1$ V/nm), the "stair" becomes smoother. The step points shift to larger wavelength (i.e., smaller photon energy) due to the lowering of the surface potential barrier by the applied dc electric field. As F_0 increases to 1 V/nm, the "stairs" still exist but the number of the "stairs" decreases and the magnitude difference between them gets smaller. When $F_1 = 0.1$ V/nm, there are two distinct "stairs" observed. Most of the emission is due to photon-assisted tunneling [cf. Figs. 1(k) and 1(l)] for relatively long laser wavelength. When $F_0 = 5$ V/nm, the electron transmission probability becomes almost independent of laser wavelength for $F_1 = 0.1$ V/nm. The dashed curve is for dc field emission without laser electric field with $F_0 = 5$ V/nm, which overlaps with the curve for $F_1 = 0.1$ V/nm. For $F_1 \geq 1$ V/nm, the dominant emission process is still direct tunneling, as shown in Figs. 1(m)–1(p). The laser electric field F_1 can modulate the emission process through photo-assisted field emission and above-threshold photoemission. It can be observed that, with a large dc field, $D(E_F)$ is larger in the relatively longer laser wavelength range, as shown in Fig. 3(d).

C. Current density and quantum efficiency

The emission current density J, calculated from Eq. (2), as a function of laser wavelength λ, is presented in Fig. 4. It should be pointed out that the laser heating effect is not considered here with the temperature T in Eq. (2) set to 300 K. Figure 4 shares similar trends as in Fig. 3 since the majority of emitted electrons originate

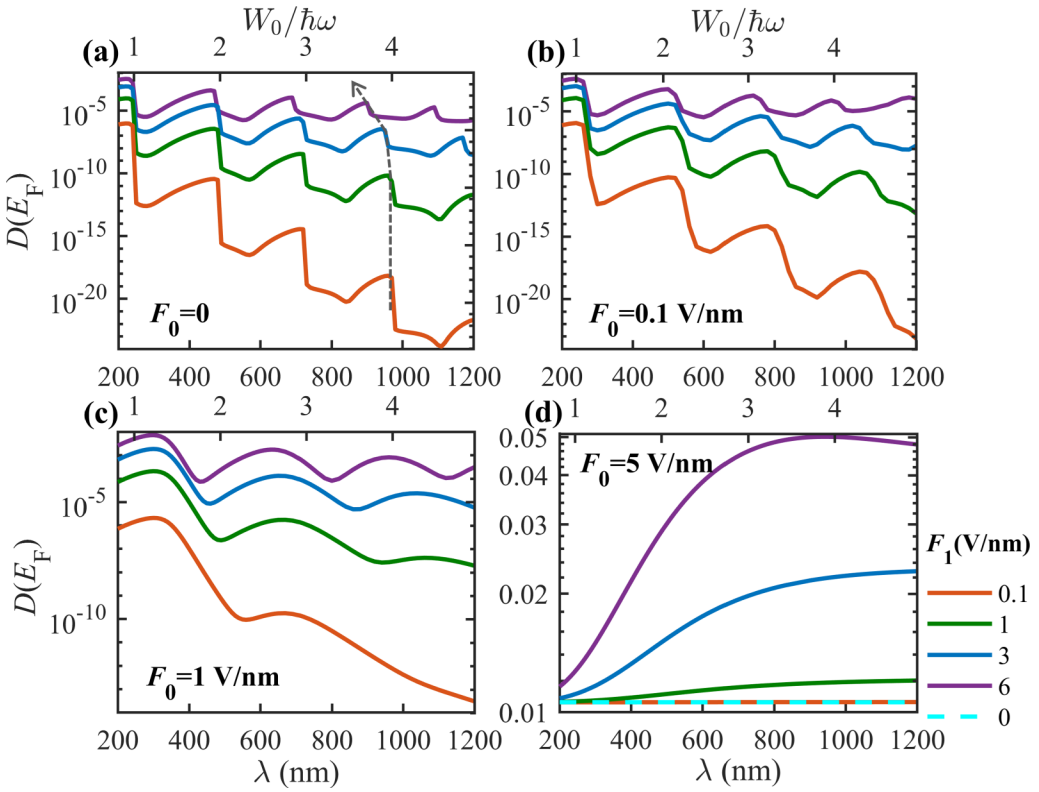

FIG. 3. Electron transmission probability $D(\varepsilon = E_F)$ with initial energy of E_F as a function of laser wavelength λ for various combinations of dc electric field F_0 and laser field F_1. (a) $F_0 = 0$; (b) $F_0 = 0.1$ V/nm; (c) $F_0 = 1$ V/nm; and (d) $F_0 = 5$ V/nm. The laser fields F_1 corresponding to solid lines in red, green, blue, purple, and the dashed line in cyan are 0.1, 1, 3, 6, and 0 V/nm, respectively.

from the vicinity of the Fermi level.[28,50] However, the curves for J vs λ are smoother than those for $D(\varepsilon = E_F)$ vs λ due to the combined emitted electrons with different initial longitudinal energies. Including a dc field will make the step edge smoother and the step point shift toward longer laser wavelength. When $F_0 = 5$ V/nm, the electron emission is increased by 1–21 orders of magnitude compared with the case of no applied dc electric field for different combinations of laser wavelength λ and laser field F_1. The dominant emission process of field emission ($n = 0$) for $F_0 = 5$ V/nm makes the emission current insensitive to the laser wavelength.

Figure 5 shows quantum efficiency (QE) as a function of laser wavelength λ and laser field strength F_1 under various dc field strengths F_0, which is calculated from Eq. (3). It is obvious that the curves for QE vs λ share similar trends as those for J vs λ in Fig. 4. For $F_0 \leq 1$ V/nm, QE is almost independent of F_1 for different laser fields $0.1\,\text{V/nm} \leq F_1 \leq 6\,\text{V/nm}$ in the smaller laser wavelength regime (or $W/\hbar\omega < 1$), which is indicated by the yellow shaded area in Figs. 5(a)–5(c). This is because the dominant single-photon photoemission in this regime follows $J \propto I = F_1^2$. Therefore, the quantum efficiency is independent of the laser field as $QE \propto J/I$. Note the majority of existing studies on QE focus only on this single-photon regime.[23,24,50] For $W_0/\hbar\omega > 1$, the photoemission is due to n-photon process, which scales as $J \propto I^n$ ($n \geq 2$), with n determined by rounding $W/\hbar\omega$ up to the nearest integer number. As a result, $QE \propto I^{n-1}$, and the quantum efficiency increases greatly as F_1 increases. As dc field increases, QE is enhanced and the step points are shifted toward longer laser wavelengths (i.e., smaller photon energy) due to the lowering of the surface potential barrier by the dc field. As a result, increasing F_0 from 0 to 1 V/nm also extends the single-photon absorption regime from ~250 to ~320 nm, where QE is independent of laser field F_1, as indicated by the yellow shaded area in Figs. 5(a)–5(c). When $F_0 = 5$ V/nm, QE can be larger than 1 due to the dominant contribution of dc field emission.

III. PHOTOEMISSION WITH LASER HEATING EFFECTS

A. Two-temperature model

It is known that electron energy distribution function (EEDF) and its dynamic due to laser heating have strong influence on photoelectron emission current and emission electron energy spectrum.[21,22,50,52,65] Electrons can be excited to higher energy levels by absorbing the laser energy. The excited electrons can come into thermal equilibrium with other electrons by electron–electron scatterings and can transfer energy to the lattice by electron–phonon scatterings. The microscopic kinetic approach, such as Boltzmann's

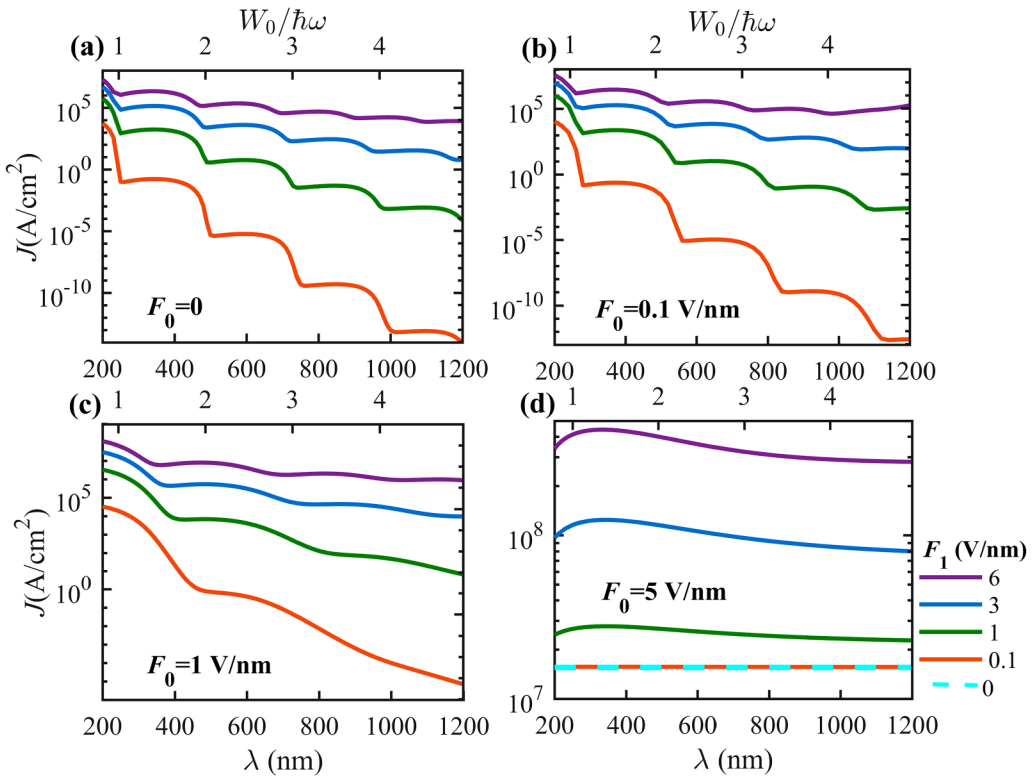

FIG. 4. Electron emission current density calculated from Eq. (2) as a function of laser wavelength λ for various combinations of dc electric field F_0 and laser field F_1. The temperature T is set to be constant at 300 K without considering laser heating. (a) $F_0 = 0$; (b) $F_0 = 0.1$ V/nm; (c) $F_0 = 1$ V/nm; and (d) $F_0 = 5$ V/nm. The laser fields F_1 corresponding to solid lines in red, green, blue, purple, and the dashed line in cyan are 0.1, 1, 3, 6, and 0 V/nm, respectively.

equation, can provide an accurate estimation of internal thermalization process and electron and phonon energy distribution, especially for femtosecond laser pulses.[29,66,67] However, the classical two-temperature model (TTM) still works well for laser pulse of ~500 fs duration[21,22,53–56] but with much lower computational complexity. We will use TTM to estimate the laser heating effects in photoemission. In TTM,[51,68] electrons and lattice are considered as two separate equilibrium subsystems, characterized by their own temperatures T_e and T_l,

$$C_e(T_e)\frac{\partial T_e(x,t)}{\partial t} = \frac{\partial}{\partial x}\kappa\frac{\partial T_e(x,t)}{\partial x} - g(T_e - T_l) + G(x,t), \quad (4a)$$

$$C_l(T_l)\frac{\partial T_l(x,t)}{\partial t} = g(T_e - T_l). \quad (4b)$$

In Eq. (4), the electron heat capacity $C_e(T_e) = \gamma T_e / \left[1 + \frac{7}{40}\left(\frac{\pi k_B T_e}{E_F}\right)^2\right]$ with k_B being the Boltzmann's constant, $\gamma = \frac{1}{3}\pi^2 k_B^2 B(\varepsilon = E_F)$ with $B(\varepsilon) = 8\pi\frac{m\eta}{(2\pi\hbar)^3}\sqrt{2m\varepsilon}$, and η an effective thermal mass term. When $k_B T_e \ll E_F$, $C_e(T_e) \approx \gamma T_e$. The lattice heat capacity $C_l(T_l) = 3Nk_B / \left[1 + \frac{1}{20}\left(\frac{T_D}{T_l}\right)^2\right]$, where N is the number density of the atoms in metal, $T_D = \frac{\hbar v_s}{k_B}(6\pi^2 Nr)^{1/3}$ is the Debye temperature, with v_s the speed of sound inside the metal and r the number of atoms per unit cell. When $T_D \ll T_l$, C_l is a constant. $g = \frac{\pi\lambda_0}{9\hbar}k_B k_F^3 m v_s^2$ is the electron–lattice coupling coefficient, where k_F is determined by the Fermi momentum $\hbar k_F = \sqrt{2mE_F}$, λ_0 is a dimensionless electron–phonon coupling constant, which is characteristic of the metal and on the order of 0.1–1. $g(T_e - T_l)$ gives the amount of energy per unit volume per unit time transferred between electron and lattice systems. $G(x,t) = I(t)P_{abs}\alpha\exp(-\alpha x)$ is the energy absorbed by the metal, where $I(t)$ is the laser intensity temporal profile, $\alpha = 4\pi k/\lambda$ is the absorption coefficient with k the extinction coefficient, the laser power absorption fraction is $P_{abs} = \pi\delta_s/\lambda$ for the parallel-to-surface incident laser,[69–71] with λ the laser wavelength in the vacuum and $\delta_s = \sqrt{2/\sigma\omega\mu_0}$ the skin depth, σ the conductivity of the metal, and μ_0 the vacuum permeability, or $P_{abs} = 1 - R$ for the incident laser tilted to the metal surface, with R the reflectivity of the laser at the metal surface. $\kappa = \frac{2E_F}{3m}C_e(T_e)\tau$ is the thermal conductivity, with τ the electron scattering time and m the electron rest mass. According to Matthiessen's rule, $\frac{1}{\tau} = \frac{1}{\tau_{e-e}} + \frac{1}{\tau_{e-ph}}$, with $\tau_{e-e} = \frac{\hbar E_F}{A_0 k_B^2}\frac{1}{T_e^2}$

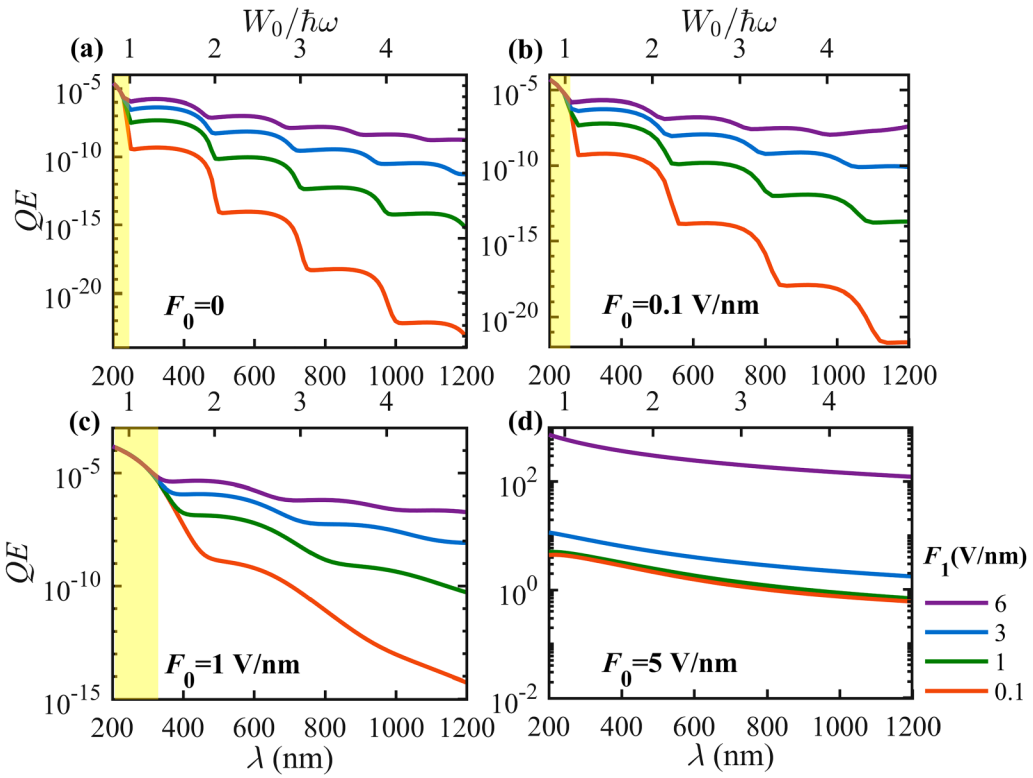

FIG. 5. Quantum efficiency (QE) calculated from Eq. (3) as a function of laser wavelength λ for various combinations of dc electric field F_0 and laser field F_1. The temperature is set to be constant at 300 K without considering laser heating. (a) $F_0 = 0$; (b) $F_0 = 0.1$ V/nm; (c) $F_0 = 1$ V/nm; and (d) $F_0 = 5$ V/nm. The laser fields F_1 corresponding to solid lines in red, green, blue, and purple, are 0.1, 1, 3, and 6 V/nm, respectively.

and $\tau_{e-ph} = \frac{\hbar}{2\pi k_B \lambda_0} \frac{1}{T_i}$ being the electron–electron and electron–phonon scattering times, respectively, and A_0 a dimensionless, material-specific quantity.

B. Electron temperature T_e

The time-dependent evolution of the electron temperature in response to an incident laser pulse with full width at half maximum (FWHM) $\tau_{FWHM} =$ 450 fs under various laser wavelengths and field strengths is shown in Figs. 6(a) and 6(b). In Fig. 6(a), the laser field strength is kept constant as $F_1 =$ 1 V/nm for laser wavelengths ranging from 200 to 1200 nm. The maximum of the electron temperature lags behind that of the incident laser intensity (dotted curve), which is centered at $t = 0$. It is interesting to find that as the laser wavelength decreases, the time delay between the maximum of the temperature and that of the laser intensity increases, and the temperature gets larger, which is due to larger laser energy absorption $G \sim k/\lambda^{3/2}$ inside the metal for parallel incidence [extinction coefficient k vs λ shown in Fig. 6(c)]. For a fixed laser wavelength ($\lambda =$ 800 nm), the electron temperature increases with the laser field strengths, as shown in Fig. 6(b). In addition, the time delay between the maximum of the electron temperature and that of the laser intensity increases. The electron temperature at $t = 0$, which corresponds to the peak of the laser intensity, and the peak electron temperature T_e^{peak}, as a function of laser wavelength are shown in Fig. 6 (d) for $F_1 =$ 1 V/nm. The temperature decreases with the laser wavelength, which is due to less absorption of the laser energy as laser wavelength increases. The obtained electron temperature T_e is then used in Eq. (2) by setting $T = T_e$ to calculate the photoemission current density.

C. Current density and quantum efficiency with laser heating

A comparison of photoemission with laser heating effects (red curves) and without laser heating effects (blue curves, with $T = T_e \equiv$ 300 K) is shown in Fig. 7. The results are taken at $t = 0$, which corresponds to the laser intensity peak [cf. the dotted curve in Fig. 6(a)]. The peak laser field strength is taken to be 1 V/nm. The electron emission current density per electron initial energy, calculated as $J(\varepsilon) = eD(\varepsilon)N(\varepsilon)$ from Eq. (2), extends to energy levels above the Fermi level as the laser heating effect is considered, as shown in Fig. 7(a) for $\lambda =$ 200, 600, and 1000 nm. This is because more electrons are excited to energy levels above the Fermi

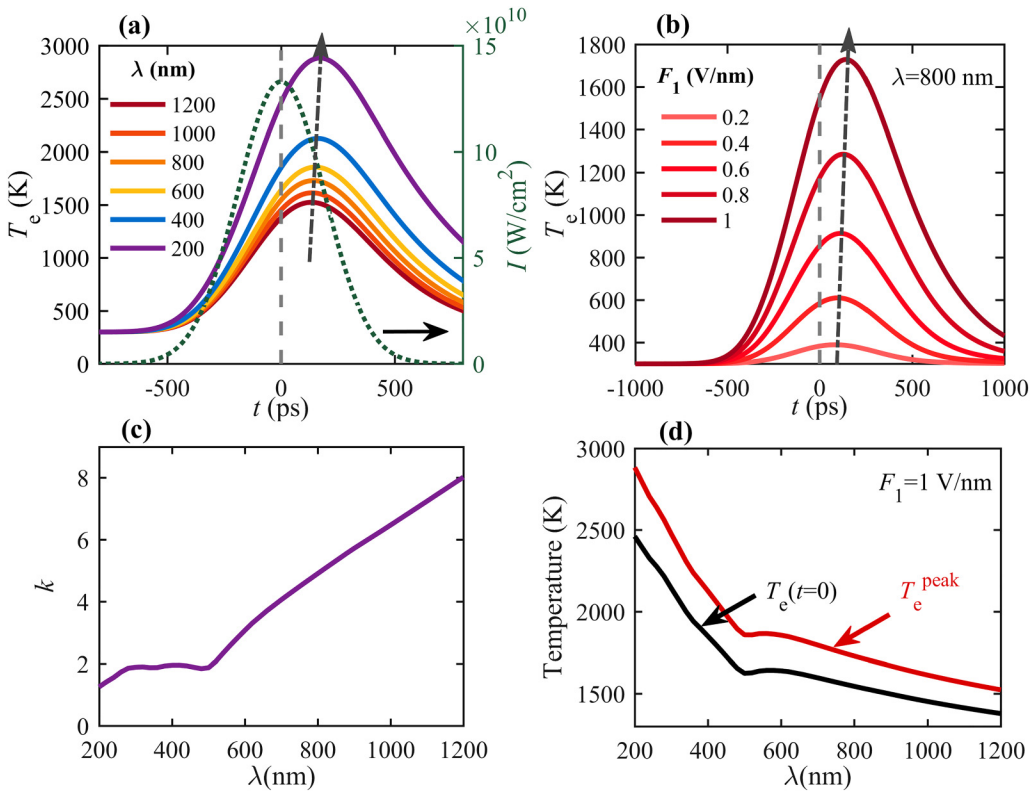

FIG. 6. Electron temperature varies with incident laser wavelength λ and laser field strength F_1 calculated from Eq. (4). (a) Electron temperature temporal profile for λ from 200 to 1200 nm with peak laser field $F_1 =$ 1 V/nm and the corresponding peak laser intensity of 1.33×10^{11} W/cm^2. The dotted curve is the laser intensity temporal profile $I(t)$. (b) Electron temperature temporal profile for peak laser field F_1 from 0.2 to 1 V/nm with $\lambda =$ 800 nm. (c) Optical constant extinction coefficient k as a function of λ.[72] (d) Electron temperature at $t =$ 0 (black curve), which corresponds to the time instant of peak laser intensity, and peak electron temperature T_e^{peak} (red curve), as a function of λ. Parameters in Eq. (4) for gold are $\eta = 1.08$, $C_l = 2.35 \times 10^6$ J/(Km^3) (assumed constant), $v_s = 3240$ m/s, $\sigma = 4.11 \times 10^7$ S/m, $A_0 = 17$, and $\lambda_0 = 0.1548$.[21,52]

level by absorbing the laser energy. The electron emission from initial energy levels above the Fermi energy accounts for 7.84%, 6.85%, and 91.1% of the total emission for $\lambda =$ 200, 600, and 1000 nm, respectively, with laser heating effects, compared to 0.13%, 0.015%, and 0.73% without laser heating. Figure 7(b) shows the emission current density as a function of the laser wavelength. The steep step point, which is the transition point between different n-photon processes, becomes smooth. This is because more electrons above the Fermi level can be emitted through smaller n-photon process, which has an emission probability orders of magnitude higher than larger n-photon process [see Figs. 1(a)–1(d) and its description in Sec. II B above]. The difference between the red and blues curves shows that the laser heating effect has a greater impact on longer wavelength laser-induced photoemission. The quantum efficiency as a function of laser wavelength is shown in Fig. 7(c), showing the same trend as J vs λ in Fig. 7(b). In summary, the increase of QE due to laser heating is the strongest near the step points (i.e., $W_0/\hbar\omega =$ integer) and is more profound for longer laser wavelengths.

D. Comparison with experimental results

We demonstrate the validity of the above quantum model with laser heating by comparing it with experimental results in Ref. 21. In the experiment, a laser pulse of 450 fs duration at 248 nm is used. The metal is copper with Fermi energy $E_F =$ 7 eV and work function $W_0 =$ 4.6 eV. The emission current density per pulse based on our quantum model[31,50] is given as

$$J_p = \frac{1}{\tau_{FWHM}} \int_{-\infty}^{\infty} J(t)dt, \tag{5}$$

where $J(t)$ is the emission current density at t calculated from Eqs. (1) and (2) and τ_{FWHM} is the full-width-half-maximum of the intensity of the laser pulse. Note that though Eq. (1) is the time-averaged transmission probability for continuous wave laser excitation, it is found to be an excellent approximation for laser pulses of longer than ten cycles.[31] Thus, it is expected to be applicable for laser pulses of 450 fs (~544 laser cycles) at 248 nm considered here.

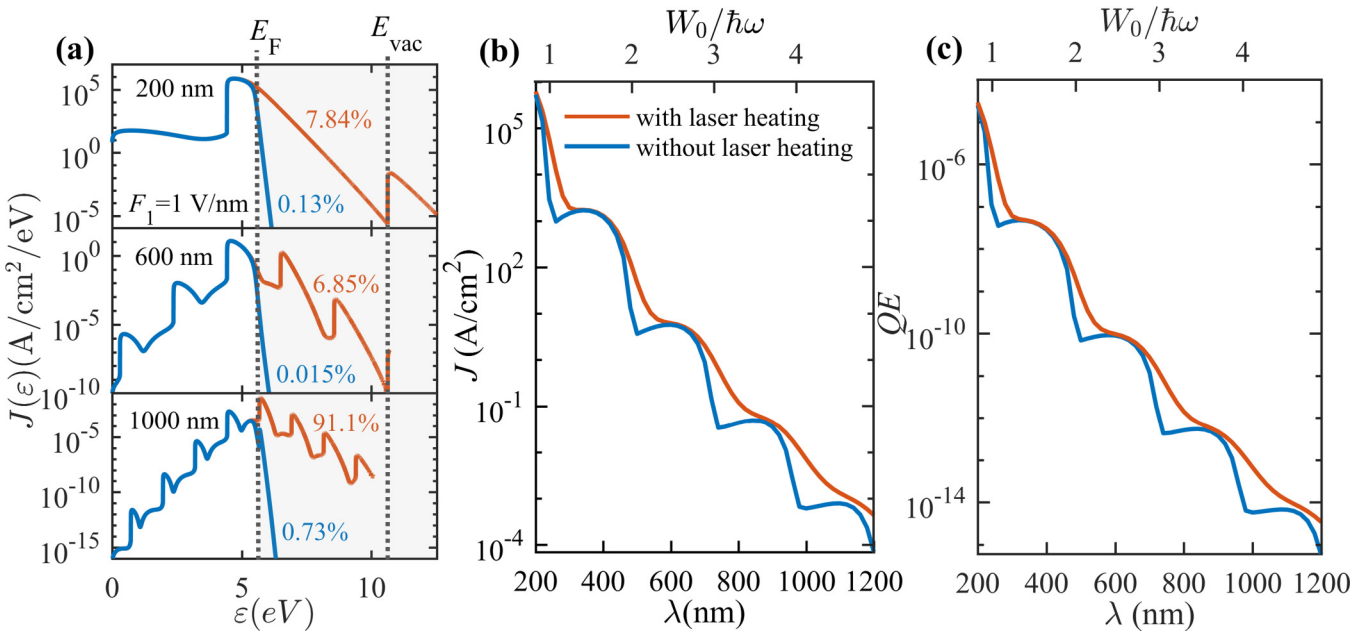

FIG. 7. Laser heating effects on photoemission. (a) Electron emission current density per electron initial energy at $t = 0$ for $\lambda =$ 200, 600, and 1000 nm with $F_1 =$ 1 V/nm and $F_0 =$ 0; (b) Electron emission current density and (c) QE at $t = 0$ as a function of laser wavelength for $F_1 =$ 1 V/nm and zero dc field $F_0 = 0$.

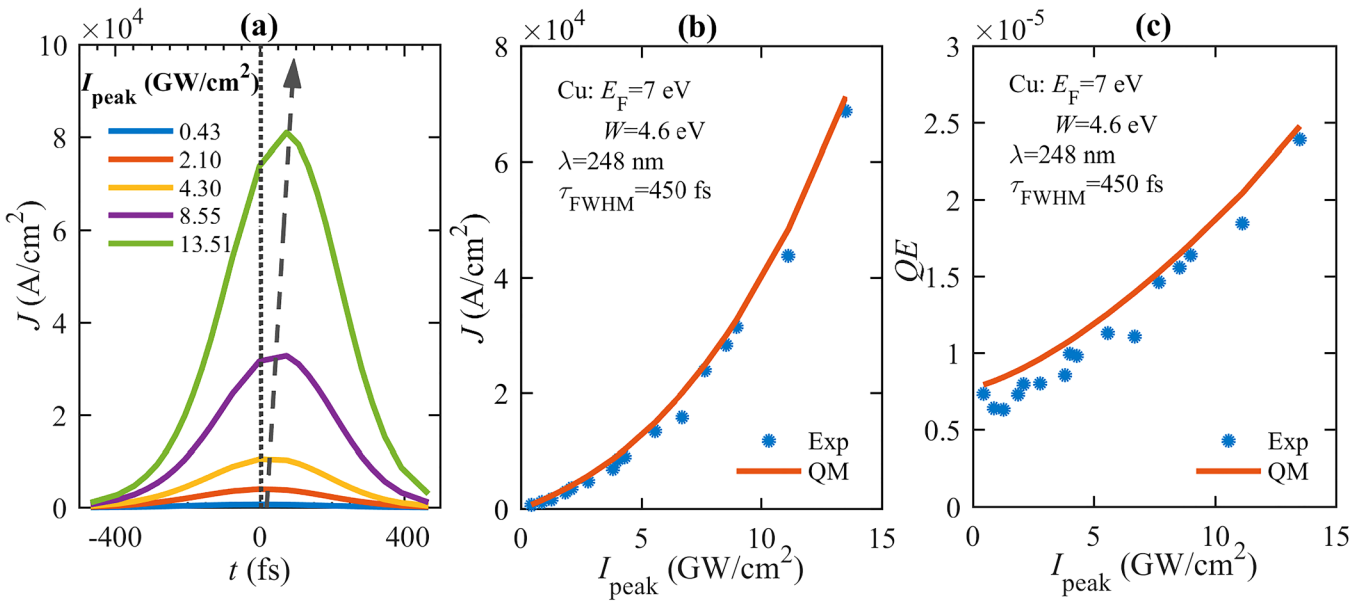

FIG. 8. Comparison with experimental results. (a) Calculated emission current density temporal profile for various laser intensities used in the experiment.[21] (b) Emission current density as a function of the peak laser intensity. Scatters are experimental data extracted from.[21] The red curve is calculated from Eq. (5) with $J(t)$ calculated by our quantum model. (c) Quantum efficiency as a function of the peak laser intensity. Parameters in Eq. (4) for copper are $\gamma = 96.6$ J/K^2/m^3, $C_l = 3.5 \times 10^6$ J/(Km^3) (assumed constant), $v_s = 5010$ m/s, $\sigma = 5.96 \times 10^7$ S/m, $A_0 k_B^2/\hbar E_F = 2.3 \times 10^7$/(K^{2}s), and $2\pi k_B \lambda_0/\hbar = 1.1 \times 10^{11}$/(Ks).[21,22,52] In the calculation, dc field $F_0 = 0$ is used; in the experiment, a dc field up to 6.6 MV/m is applied to overcome the space-charge effect.

The temporal profile of the emission current density is shown in Fig. 8(a). As the laser intensity increases, the emission current density increases, and the current density peak lags behind the laser intensity peak. This is due to the delay between the temperature peak and the laser intensity peak, as shown in Figs. 6(a) and 6(b), which has also been observed in Ref. 73. The calculated current density by the quantum model from Eq. (5) is shown as red curve in Fig. 8(b), which is in good agreement with the experimental measured current density shown as blue scatter points in Fig. 8(b). The small difference can be ascribed to the different settings of the experiment and our quantum model. In the experiment, the laser field is incident onto the metal surface with an angle of 80° to the normal. However, in our model, the laser field is perpendicular to metal surface (i.e., parallel incidence). For n-photon absorption process, the emission current density $J \propto (F_1 \cos\theta)^{2n}$ with θ being the angle between field polarization and the normal of the cathode surface.[27] Therefore, our model slightly overestimates the photoemission. The quantum efficiency is plotted in Fig. 8(c). To be consistent with the current density Eq. (5), the laser intensity I in Eq. (3) is calculated by $I = \int_{-\infty}^{\infty} I(t)dt/\tau_{FWHM}$ in order to calculate QE. It is clear that QE increases with the laser intensity instead of being constant as shown in Figs. 5(a)–5(c) at 248 nm, which is ascribed to the laser heating induced electron redistribution.

IV. CONCLUSION

In summary, we have analyzed photoemission from metal surfaces with the laser wavelength from 200 to 1200 nm (i.e., UV to NIR), based on an analytical quantum model by solving the time-dependent Schrödinger equation. The photoemission mechanisms vary from multiphoton absorption to dc or optical field emission,[74] depending on the laser wavelength and intensity, and dc electric field. When $F_0 \leq 0.1$ V/nm, which is much smaller than the typical dc field used in static field emission, the emission current density and quantum efficiency (QE) are characterized by different n-photon absorption processes. Channel closing effects and more above-threshold photoemission ($n > W/\hbar\omega$) are observed as the laser field increases, especially for longer wavelengths. It is found that QE in the short wavelength regime (or single-photon regime, $n = 1$) is insensitive to the laser field strength for $F_0 \leq 1$ V/nm. When $F_0 = 5$ V/nm, the static field emission ($n = 0$) becomes dominant, regardless of the laser wavelength (200 nm $\leq \lambda \leq$ 1200 nm) and the laser field strength (0.1 V/nm $\leq F_1 \leq$ 6 V/nm).

Laser heating induced electron dynamics is considered by using two-temperature model (TTM), which is applicable for sub-picosecond laser pulses. The electron temperature rise shows a strong dependence on the laser wavelength. It is found that QE increases nonlinearly with the laser intensity for sub-picosecond laser pulses. The increase is the strongest near wavelengths where the work function of the metal is integer multiple of the corresponding photon energy. The quantum model with the laser heating included also reproduce previous experimental results, which further validates our quantum model and the importance of laser heating.

The quantum model is one dimensional without considering the cathode geometry, surface roughness, and the field enhancement. It is expected to be valid for cathodes of various shapes by considering the corresponding local field enhancement and local surface conditions.[57,59,75] While our model is derived for continuous wave excitation, it is still a good approximation to laser pulses of longer than ten cycles.[31] As the laser pulse duration further decreases, a model for few-cycle pulsed laser-induced photoemission is demanded.[11] In that case, TTM may fail due to the thermal non-equilibrium in both the electron and lattice systems. The microscopic kinetic theory, such as Boltzmann's equation,[65–67] needs to be used. The consistent treatment of the dynamic electron energy distribution function and electron emission, induced by a laser pulse of a few to a hundred femtoseconds, will be the subject of future study.

ACKNOWLEDGMENTS

This work was supported by the Air Force Office of Scientific Research (AFOSR) YIP Award (No. FA9550-18-1-0061) and the Office of Naval Research (ONR) YIP (Grant No. N00014-20-1-2681).

DATA AVAILABILITY

The data that support the findings of this study are available from the corresponding author upon reasonable request.

REFERENCES

[1]C. A. Brau, "High-brightness electron beams—Small free-electron lasers," Nucl. Instrum. Methods Phys. Res. A **407**, 1 (1998).
[2]P. G. O'Shea and H. P. Freund, "Free-electron lasers: Status and applications," Science **292**, 1853 (2001).
[3]I. Grguraš, A. R. Maier, C. Behrens, T. Mazza, T. J. Kelly, P. Radcliffe, S. Düsterer, A. K. Kazansky, N. M. Kabachnik, T. Tschentscher, J. T. Costello, M. Meyer, M. C. Hoffmann, H. Schlarb, and A. L. Cavalieri, "Ultrafast x-ray pulse characterization at free-electron lasers," Nat. Photonics **6**, 852 (2012).
[4]K. L. Jensen and E. J. Montgomery, "Photoemission theory and the development of high performance photocathodes," J. Comput. Theor. Nanosci. **6**, 1754 (2009).
[5]J. S. Kim, T. LaGrange, B. W. Reed, M. L. Taheri, M. R. Armstrong, W. E. King, N. D. Browning, and G. H. Campbell, "Imaging of transient structures using nanosecond *in situ* TEM," Science **321**, 1472 (2008).
[6]A. H. Zewail, "Four-dimensional electron microscopy," Science **328**, 187 (2010).
[7]A. Feist, K. E. Echternkamp, J. Schauss, S. V. Yalunin, S. Schäfer, and C. Ropers, "Quantum coherent optical phase modulation in an ultrafast transmission electron microscope," Nature **521**, 200 (2015).
[8]S. Sun, X. Sun, D. Bartles, E. Wozniak, J. Williams, P. Zhang, and C.-Y. Ruan, "Direct imaging of plasma waves using ultrafast electron microscopy," Struct. Dyn. **7**, 064301 (2020).
[9]A. Feist, N. Bach, N. Rubiano da Silva, T. Danz, M. Möller, K. E. Priebe, T. Domröse, J. G. Gatzmann, S. Rost, J. Schauss, S. Strauch, R. Bormann, M. Sivis, S. Schäfer, and C. Ropers, "Ultrafast transmission electron microscopy using a laser-driven field emitter: Femtosecond resolution with a high coherence electron beam," Ultramicroscopy **176**, 63 (2017).
[10]B. Piglosiewicz, S. Schmidt, D. J. Park, J. Vogelsang, P. Groß, C. Manzoni, P. Farinello, G. Cerullo, and C. Lienau, "Carrier-envelope phase effects on the strong-field photoemission of electrons from metallic nanostructures," Nat. Photonics **8**, 37 (2014).
[11]Y. Luo, Y. Zhou, and P. Zhang, "Few-cycle optical-field-induced photoemission from biased surfaces: An exact quantum theory," Phys. Rev. B **103**, 085410 (2021).

[12]P. Dombi, Z. Pápa, J. Vogelsang, S. V. Yalunin, M. Sivis, G. Herink, S. Schäfer, P. Groß, C. Ropers, and C. Lienau, "Strong-field nano-optics," Rev. Mod. Phys. **92**, 025003 (2020).
[13]P. Dombi, A. Hörl, P. Rácz, I. Márton, A. Trügler, J. R. Krenn, and U. Hohenester, "Ultrafast strong-field photoemission from plasmonic nanoparticles," Nano Lett. **13**, 674 (2013).
[14]P. Rácz, Z. Pápa, I. Márton, J. Budai, P. Wróbel, T. Stefaniuk, C. Prietl, J. R. Krenn, and P. Dombi, "Measurement of nanoplasmonic field enhancement with ultrafast photoemission," Nano Lett. **17**, 1181 (2017).
[15]E. Forati, T. J. Dill, A. R. Tao, and D. Sievenpiper, "Photoemission-based microelectronic devices," Nat. Commun. **7**, 13399 (2016).
[16]P. Zhang and Y. Y. Lau, "Ultrafast and nanoscale diodes," J. Plasma Phys. **82**, 595820505 (2016).
[17]P. Zhang, Á Valfells, L. K. Ang, J. W. Luginsland, and Y. Y. Lau, "100 years of the physics of diodes," Appl. Phys. Rev. **4**, 011304 (2017).
[18]C. Karnetzky, P. Zimmermann, C. Trummer, C. Duque Sierra, M. Wörle, R. Kienberger, and A. Holleitner, "Towards femtosecond on-chip electronics based on plasmonic hot electron nano-emitters," Nat. Commun. **9**, 2471 (2018).
[19]F. Rezaeifar, H. U. Chae, R. Ahsan, and R. Kapadia, "Hot electron emission from waveguide integrated lanthanum hexaboride nanoparticles," Appl. Phys. Lett. **118**, 071108 (2021).
[20]P. Zhang, Y. S. Ang, A. L. Garner, A. Valfells, J. W. Luginsland, and L. K. Ang, "Space-charge limited current in nanodiodes: Ballistic, collisional and dynamical effects," J. Appl. Phys. **129**, 100902 (2021).
[21]N. A. Papadogiannis, S. D. Moustaïzis, and J. P. Girardeau-Montaut, "Electron relaxation phenomena on a copper surface via nonlinear ultrashort single-photon photoelectric emission," J. Phys. D: Appl. Phys. **30**, 2389 (1997).
[22]N. A. Papadogiannis and S. D. Moustaizis, "Ultrashort laser-induced electron photoemission: A method to characterize metallic photocathodes," J. Phys. D: Appl. Phys. **34**, 499 (2001).
[23]D. H. Dowell, F. K. King, R. E. Kirby, J. F. Schmerge, and J. M. Smedley, "*In situ* cleaning of metal cathodes using a hydrogen ion beam," Phys. Rev. Spec. Top. Accel. Beams **9**, 063502 (2006).
[24]D. H. Dowell and J. F. Schmerge, "Quantum efficiency and thermal emittance of metal photocathodes," Phys. Rev. Spec. Top. Accel. Beams **12**, 074201 (2009).
[25]D. Novko, V. Despoja, M. Reutzel, A. Li, H. Petek, and B. Gumhalter, "Plasmonically assisted channels of photoemission from metals," Phys. Rev. B **103**, 205401 (2021).
[26]P. Hommelhoff, Y. Sortais, A. Aghajani-Talesh, and M. A. Kasevich, "Field emission tip as a nanometer source of free electron femtosecond pulses," Phys. Rev. Lett. **96**, 077401 (2006).
[27]B. Barwick, C. Corder, J. Strohaber, N. Chandler-Smith, C. Uiterwaal, and H. Batelaan, "Laser-induced ultrafast electron emission from a field emission tip," New J. Phys. **9**, 142 (2007).
[28]M. Schenk, M. Krüger, and P. Hommelhoff, "Strong-field above-threshold photoemission from sharp metal tips," Phys. Rev. Lett. **105**, 257601 (2010).
[29]M. Pant and L. K. Ang, "Ultrafast laser-induced electron emission from multi-photon to optical tunneling," Phys. Rev. B **86**, 045423 (2012).
[30]M. R. Bionta, S. J. Weber, I. Blum, J. Mauchain, B. Chatel, and B. Chalopin, "Wavelength and shape dependent strong-field photoemission from silver nanotips," New J. Phys. **18**, 103010 (2016).
[31]P. Zhang and Y. Y. Lau, "Ultrafast strong-field photoelectron emission from biased metal surfaces: Exact solution to time-dependent Schrödinger equation," Sci. Rep. **6**, 19894 (2016).
[32]Y. Luo and P. Zhang, "Ultrafast strong-field photoelectron emission due to two-color laser fields," Phys. Rev. B **98**, 165442 (2018).
[33]D. J. Park, B. Piglosiewicz, S. Schmidt, H. Kollmann, M. Mascheck, and C. Lienau, "Strong field acceleration and steering of ultrafast electron pulses from a sharp metallic nanotip," Phys. Rev. Lett. **109**, 244803 (2012).
[34]G. Herink, D. R. Solli, M. Gulde, and C. Ropers, "Field-driven photoemission from nanostructures quenches the quiver motion," Nature **483**, 190 (2012).
[35]L. Wimmer, G. Herink, D. R. Solli, S. V. Yalunin, K. E. Echternkamp, and C. Ropers, "Terahertz control of nanotip photoemission," Nat. Phys. **10**, 432 (2014).
[36]R. H. Fowler, "The analysis of photoelectric sensitivity curves for clean metals at various temperatures," Phys. Rev. **38**, 45 (1931).
[37]L. A. DuBridge, "A further experimental test of Fowler's theory of photoelectric emission," Phys. Rev. **39**, 108 (1932).
[38]L. A. DuBridge, "Theory of the energy distribution of photoelectrons," Phys. Rev. **43**, 727 (1933).
[39]W. E. Spicer, "Photoemissive, photoconductive, and optical absorption studies of alkali-antimony compounds," Phys. Rev. **112**, 114 (1958).
[40]C. N. Berglund and W. E. Spicer, "Photoemission studies of copper and silver: Theory," Phys. Rev. **136**, A1030 (1964).
[41]W. F. Krolikowski and W. E. Spicer, "Photoemission studies of the noble metals. I. Copper," Phys. Rev. **185**, 882 (1969).
[42]W. F. Krolikowski and W. E. Spicer, "Photoemission studies of the noble metals. II. Gold," Phys. Rev. B **1**, 478 (1970).
[43]J. H. Bechtel, W. L. Smith, and N. Bloembergen, "Four-photon photoemission from tungsten," Opt. Commun. **13**, 56 (1975).
[44]J. H. Bechtel, W. Lee Smith, and N. Bloembergen, "Two-photon photoemission from metals induced by picosecond laser pulses," Phys. Rev. B **15**, 4557 (1977).
[45]G. Ferrini, F. Banfi, C. Giannetti, and F. Parmigiani, "Non-linear electron photoemission from metals with ultrashort pulses," Nucl. Instrum. Methods Phys. Res. A **601**, 123 (2009).
[46]W. Wendelen, D. Autrique, and A. Bogaerts, "Space charge limited electron emission from a Cu surface under ultrashort pulsed laser irradiation," Appl. Phys. Lett. **96**, 051121 (2010).
[47]W. Wendelen, B. Y. Mueller, D. Autrique, B. Rethfeld, and A. Bogaerts, "Space charge corrected electron emission from an aluminum surface under non-equilibrium conditions," J. Appl. Phys. **111**, 113110 (2012).
[48]L. V. Keldysh, "Ionization in the field of a strong electromagnetic wave," Sov. Phys. JETP **20**, 1307 (1965).
[49]S. V. Yalunin, M. Gulde, and C. Ropers, "Strong-field photoemission from surfaces: Theoretical approaches," Phys. Rev. B **84**, 195426 (2011).
[50]Y. Zhou and P. Zhang, "A quantum model for photoemission from metal surfaces and its comparison with the three-step model and Fowler–DuBridge model," J. Appl. Phys. **127**, 164903 (2020).
[51]S. I. Anisimov, B. L. Kapeliovich, and T. L. Perel'man, "Electron emission from metal surfaces exposed to ultrashort laser pulses," Zh. Eksp. Teor. Fiz. **66**, 776 (1974).
[52]K. L. Jensen, D. W. Feldman, N. A. Moody, and P. G. O'Shea, "A photoemission model for low work function coated metal surfaces and its experimental validation," J. Appl. Phys. **99**, 124905 (2006).
[53]R. H. M. Groeneveld, R. Sprik, and A. Lagendijk, "Femtosecond spectroscopy of electron-electron and electron-phonon energy relaxation in Ag and Au," Phys. Rev. B **51**, 11433 (1995).
[54]J. Hohlfeld, S.-S. Wellershoff, J. Güdde, U. Conrad, V. Jähnke, and E. Matthias, "Electron and lattice dynamics following optical excitation of metals," Chem. Phys. **251**, 237 (2000).
[55]S. Tsujino, P. Beaud, E. Kirk, T. Vogel, H. Sehr, J. Gobrecht, and A. Wrulich, "Ultrafast electron emission from metallic nanotip arrays induced by near infrared femtosecond laser pulses," Appl. Phys. Lett. **92**, 193501 (2008).
[56]K. Vestentoft and P. Balling, "Formation of an extended nanostructured metal surface by ultra-short laser pulses: Single-pulse ablation in the high-fluence limit," Appl. Phys. A **84**, 207 (2006).
[57]Y. Luo and P. Zhang, "Analysis of two-color laser-induced electron emission from a biased metal surface using an exact quantum mechanical solution," Phys. Rev. Appl. **12**, 044056 (2019).
[58]Y. Luo, J. Luginsland, and P. Zhang, "Interference modulation of photoemission from biased metal cathodes driven by two lasers of the same frequency," AIP Adv. **10**, 075301 (2020).
[59]X. Xiong, Y. Zhou, Y. Luo, X. Li, M. Bosman, L. K. Ang, P. Zhang, and L. Wu, "Plasmon-enhanced resonant photoemission using atomically thick dielectric coatings," ACS Nano **14**, 8806 (2020).

[60]S. Coulombe and J.-L. Meunier, "Thermo-field emission: A comparative study," J. Phys. D: Appl. Phys. **30**, 776 (1997).
[61]J. G. Simmons, "Generalized formula for the electric tunnel effect between similar electrodes separated by a thin insulating film," J. Appl. Phys. **34**, 1793 (1963).
[62]P. Zhang, "Scaling for quantum tunneling current in nano- and subnano-scale plasmonic junctions," Sci. Rep. **5**, 9826 (2015).
[63]S. Banerjee and P. Zhang, "A generalized self-consistent model for quantum tunneling current in dissimilar metal-insulator-metal junction," AIP Adv. **9**, 085302 (2019).
[64]F. H. M. Faisal, J. Z. Kamiński, and E. Saczuk, "Photoemission and high-order harmonic generation from solid surfaces in intense laser fields," Phys. Rev. A **72**, 023412 (2005).
[65]M. Pant and L. K. Ang, "Time-dependent quantum tunneling and nonequilibrium heating model for the generalized Einstein photoelectric effect," Phys. Rev. B **88**, 195434 (2013).
[66]L. Wu and L. K. Ang, "Nonequilibrium model of ultrafast laser-induced electron photofield emission from a dc-biased metallic surface," Phys. Rev. B **78**, 224112 (2008).
[67]L. K. Ang and M. Pant, "Generalized model for ultrafast laser induced electron emission from a metal tip," Phys. Plasmas **20**, 056705 (2013).
[68]W. S. Fann, R. Storz, H. W. K. Tom, and J. Bokor, "Direct measurement of nonequilibrium electron-energy distributions in subpicosecond laser-heated gold films," Phys. Rev. Lett. **68**, 2834 (1992).
[69]S. Ramo, J. R. Whinnery, and T. Van Duzer, *Fields and Waves in Communication Electronics*, 3rd ed. (Wiley, New York, 1994).
[70]P. Zhang, Y. Y. Lau, and R. M. Gilgenbach, "Analysis of radio-frequency absorption and electric and magnetic field enhancements due to surface roughness," J. Appl. Phys. **105**, 114908 (2009).
[71]C. Pérez-Arancibia, P. Zhang, O. P. Bruno, and Y. Y. Lau, "Electromagnetic power absorption due to bumps and trenches on flat surfaces," J. Appl. Phys. **116**, 124904 (2014).
[72]P. B. Johnson and R. W. Christy, "Optical constants of the noble metals," Phys. Rev. B **6**, 4370 (1972).
[73]H. Yanagisawa, M. Hengsberger, D. Leuenberger, M. Klöckner, C. Hafner, T. Greber, and J. Osterwalder, "Energy distribution curves of ultrafast laser-induced field emission and their implications for electron dynamics," Phys. Rev. Lett. **107**, 087601 (2011).
[74]S. Zhou, K. Chen, M. T. Cole, Z. Li, J. Chen, C. Li, and Q. Dai, "Ultrafast field-emission electron sources based on nanomaterials," Adv. Mater. **31**, 1805845 (2019).
[75]Y. Zhou and P. Zhang, "Theory of field emission from dielectric coated surfaces," Phys. Rev. Res. **2**, 043439 (2020).